A hybrid data driven framework considering feature extraction for battery state of health estimation and remaining useful life prediction.

CHEN, Y., DUAN, W., HE, Y. WANG, S. and FERNANDEZ, C.

2024

Green Energy and Intelligent Transportation 3 (2024) 100160

Contents lists available at ScienceDirect

Green Energy and Intelligent Transportation

journal homepage: www.journals.elsevier.com/green-energy-and-intelligent-transportation

Full length article

A hybrid data driven framework considering feature extraction for battery state of health estimation and remaining useful life prediction

Yuan Chen [a], Wenxian Duan [b,*], Yigang He [c,**], Shunli Wang [d], Carlos Fernandez [e]

[a] School of Artificial Intelligence, Anhui University, Hefei 230009, China
[b] State Key Laboratory of Automotive Simulation and Control, Jilin University, Changchun 130022, China
[c] School of Electrical Engineering and Automation, Wuhan University, Wuhan 430000, China
[d] School of Information Engineering, Southwest University of Science and Technology, Mianyang 621010, China
[e] School of Pharmacy and Life Sciences, Robert Gordon University, Aberdeen, AB10-7GJ, UK

HIGHLIGHTS

- A hybrid framework considering feature extraction is proposed to achieve a more accurate and stable prediction performance.
- The framework combines variational mode decomposition, the multi-kernel support vector regression model and the optimization algorithm.
- Elite chaotic opposition-learning strategy and adaptive weights are introduced to optimize the sparrow search algorithm.

GRAPHICAL ABSTRACT

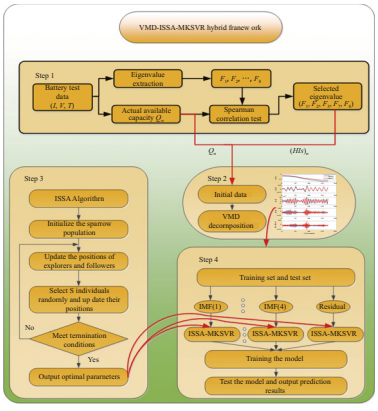

ARTICLE INFO

Keywords:
State of heath
Improved sparrow search algorithm
Remaining useful life
Variational mode decomposition
Multi-kernel support vector regression
Feature extraction

ABSTRACT

Battery life prediction is of great significance to the safe operation, and reduces the maintenance costs. This paper proposes a hybrid framework considering feature extraction to achieve more accurate and stable life prediction performance of the battery. By feature extraction, eight features are obtained to fed into the life prediction model. The hybrid framework combines variational mode decomposition, the multi-kernel support vector regression model and the improved sparrow search algorithm to solve the problem of data backward, uneven distribution of high-dimensional feature space and the local escape ability, respectively. Better parameters of the estimation model are obtained by introducing the elite chaotic opposition-learning strategy and adaptive weights to optimize the sparrow search algorithm. The algorithm can improve the local escape ability and convergence performance and find the global optimum. The comparison is conducted by dataset from National Aeronautics and Space Administration which shows that the proposed framework has a more accurate and stable prediction performance. Compared with other algorithms, the SOH estimation accuracy of the proposed algorithm is improved by 0.16%–1.67%. With the advance of the start point, the RUL prediction accuracy of the proposed algorithm does not change much.

* Corresponding author.
** Corresponding author.
E-mail address: dwx342977542@126.com (W. Duan).

https://doi.org/10.1016/j.geits.2024.100160
Received 2 August 2023; Received in revised form 20 September 2023; Accepted 27 September 2023
Available online 10 January 2024

1. Introduction

Lithium-ion batteries have the characteristics of high energy density and long cycle life, and are now widely used in electric vehicles, mobile phones, laptops and other electronic products [1]. As the number of charges and discharges increases, the battery performance continues to decline, manifested by a decrease in capacity and an increase in internal resistance. It is characterized by state of health (SOH) and remaining useful life (RUL) [2–4]. In this paper, the ratio of the current available capacity to the rated capacity of the battery is used to express the battery. The expression of SOH is as follows:

$$SOH_n = Q_n / Q_N \tag{1}$$

where, Q_n represents the actual battery capacity during the n^{th} charging and discharging cycle; Q_N represents the rated battery capacity. RUL prediction reflects the long-term battery life prediction, which can ensure its safety and stability during the whole life cycle and provide information for battery replacement. Battery capacity is easier to measure and more meaningful than impedance or internal resistance, which is adopted as the SOH definition in this study.

1.1. Literature review

Battery SOH estimation and RUL prediction methods are divided into model-based and data-driven methods [5]. Model-based methods can achieve life prediction though different models combined with the filtering algorithm such as unscented Kalman filter (UKF) algorithm, particle filter (PF) algorithm and some improved PF algorithms [6–9]. Dual exponential model is the most commonly used model. As the number of iterations increases, the diversity of particles will disappear and lead to the phenomenon of particle degradation. Improvement of importance density function and resampling method can solve this problem and improve the prediction accuracy [10–13]. In literature [14], a framework combined improved ant lion optimization algorithm and support vector regression is proposed to solve the degeneracy phenomenon of the standard PF method. It achieves prediction results with high accuracy and robustness. The PF and improved PF algorithms have good prediction accuracy and can describe the uncertainty of the battery with the probability distribution function (PDF). However, model-based methods depend on the battery capacity model, while there is no accurate and universal model, the results will be affected. Data-driven methods such as artificial neural networks (ANN) algorithm [15–17], long short-term memory neural network (LSTM) [18] and support vector machines (SVM) algorithm [19–22] have received widespread attention at present. A new framework combined partial incremental capacity and ANN is proposed in Ref. [23] for battery life prediction to get a good performance with better generalization ability and higher prediction accuracy. However, lots of data and time are needed to train the ANN models. SVM as a kind of machine learning algorithms, can be used for recognition and classification. The efficiency of regression convergence is higher than other machine learning algorithms and suitable for small sample prediction. Zhao et al. [24] develops a method combining the feature vector and SVR algorithms for battery SOH estimation. Although the prediction accuracy is higher than that of standard SVR algorithm, it still fails to solve the problem of super parameter optimization. Hybrid algorithms of SVR model and parameter optimization algorithms can make better use of their respective advantages and overcome the limitations of SVR model [25–27]. In Ref. [28], the particle swarm optimization (PSO) is applied to obtain optimized parameters of SVR model for a better battery RUL prediction. However, PSO algorithm cannot handle discrete optimization problems well and easily lead to local optimization. An artificial bee colony (ABC) algorithm is designed in Ref. [29] to identify the parameters of SVR model to solve the problem of local optimization and improves the prediction accuracy to a certain extent. In addition, in actual operation situation, the battery is affected by a lot of noise produced by its own physical characteristics and the environment, which is not considered in many articles. In order to reduce this random noise interference, research on signal processing methods are conducted. In Ref. [30], the empirical model decomposition (EMD) algorithm is proposed to decompose the non-stationary signals for noise reduction. However, the EMD method exists the problems of end effect and modal component. The variational mode decomposition (VMD) can overcome problems above to reduce the non-stationarity of time series.

1.2. Contributions of this paper

In this study, a hybrid framework considering feature extraction is proposed for a better SOH estimation and RUL prediction performance. The hybrid framework combining VMD, improved sparrow search algorithm (ISSA) and multi-kernel support vector regression (MKSVR) model. The contributions are summarized. First, eight features are obtained to fed into the life prediction model by feature extraction. Secondly, VMD method is applied to decompose the original data to make the capacity data more stable. Then, elite chaotic opposition-learning strategy and adaptive weights are adopted to optimize the traditional sparrow search algorithm (SSA) to obtain more accurate parameters of the prediction model. Finally, MKSVR is used to solve the low prediction accuracy problem caused by large sample data and uneven distribution of high-dimensional feature space.

1.3. Organization of the paper

The remainder of this article is listed as follows. Section 2 introduces the VMD decomposition, the MKSVR model, the ISSA algorithm for parameters optimization and the hybrid VMD-ISSA-MKSVR framework. Section 3 discusses experimental results and analysis of the proposed method. Conclusions are summarized in Section 4.

2. Basic theories

2.1. Variational mode decomposition

VMD is used for completely non-recursive modal variation to deal with signals [31,32]. The optimal solution of the variational problem is obtained finally by effective decomposition component of the given signal. By iteration, the VMD algorithm can decompose the signals into some intrinsic mode functions (IMFs) and a relevant residual value containing multiple different frequency scales.

The constrained variational expression of VMD is as follows:

$$\begin{aligned} &\min_{\{Q_m\},\{\omega_m\}} \left\{ \sum_{m=1}^{M} \left\| \partial_N \left[(\delta(N) + j/\pi N) * Q_m(N) \right] \exp(-j\omega_m N) \right\|_2^2 \right\}, \\ &s.t. \sum_{m=1}^{M} Q_m = f \end{aligned} \tag{2}$$

where M is the number of modes to be decomposed,$\{Q_m\} = \{Q_1,Q_2,\cdots,Q_m\}$ is the set of M modal components after decomposition, $\{\omega_m\} = \{\omega_1,\omega_2,\cdots,\omega_m\}$ is the set of center frequencies corresponding to modal component, Q_m is the m-th modal component, ω_m is the center frequency of m-th modal component, N is the number of sequences, $\delta(t)$ represents the dirac function.

The unconstrained variational expression is shown below by introducing the Lagrangian multiplication operator λ:

$$\begin{aligned} L(\{Q_m\},\{\omega_m\}) = \alpha \sum_{m=1}^{M} \left\| \partial_N \left[(\delta(N) + j/\pi N) * Q_m(N) \right] \exp(-j\omega_m N) \right\|_2^2 + \left\| f(N) \right. \\ \left. - \sum_m Q_m(N) \right\|_2^2 + \langle \lambda(N), f(N) - \sum_m Q_m(N) \rangle \end{aligned} \tag{3}$$

where α is a secondary penalty factor.

By alternating direction multiplier iterative algorithm to obtain M modal components, the unconstrained variational problem can be solved. The update expressions of Q_m, ω_m and λ are shown as follows:

$$\begin{aligned}\widehat{Q}_m^{k+1}(\omega) &= \frac{\widehat{f}(\omega) - \sum_{i=1}^{m}\widehat{Q}_i^{k+1}(\omega) - \sum_{i=m+1}^{M} Q_i^k(\omega) + \widehat{\lambda}(\omega)/2}{1 + 2\alpha(\omega - \omega_m^k)^2} \\ \omega_m^{k+1} &= \frac{\int_0^\infty \omega\left|\widehat{Q}_m^{k+1}(\omega)\right|^2 \mathrm{d}\omega}{\int_0^\infty \left|\widehat{Q}_m^{k+1}(\omega)\right|^2 \mathrm{d}\omega} \\ \widehat{\lambda}^{k+1}(\omega) &= \widehat{\lambda}^k(\omega) + \gamma\left(\widehat{f}(\omega) - \sum_{m=1}^{M}\widehat{Q}_m^{k+1}(\omega)\right)\end{aligned} \tag{4}$$

where γ is the update coefficient for Lagrangian multiplier which represents noise tolerance. $\widehat{Q}_m(\omega)$, $\widehat{Q}_i(\omega)$, $\widehat{f}(\omega)$ and $\widehat{\lambda}(\omega)$ are Fourier transforms of $\widehat{Q}_m$, $\widehat{Q}_i$, $\widehat{f}$ and $\widehat{\lambda}$.

The process of VMD algorithm is summarized as follows:

Step 1. Initialize three parameters $\widehat{Q}_m^1$, ω_m^1, $\widehat{\lambda}^1$ and set the iteration count to $k = 1$.

Step 2. Update $\widehat{Q}_m$ ω_m and $\widehat{\lambda}$ by Eq. (4).

Step 3. For a specified acceptable tolerance ξ>0, the convergence criterion is $\sum_{m=1}^{M}\left\|\widehat{Q}_m^{k+1}(\omega) - \widehat{Q}_m^k(\omega)\right\|_2^2 / \left\|\widehat{Q}_m^k(\omega)\right\|_2^2 < \xi$. If the convergence is realized, finish the iteration and output the final value, else return to step 2.

2.2. Multi-kernel support vector regression

In 1995, SVM algorithm based on statistical learning theory was proposed by Vapnik. It is mainly used to obtain the global optimal solution for pattern recognition and classification. To reduce the parameter dimension, the optimization process is simplified by introducing the kernel function. When used as a regression tool, SVM implements a variant of the algorithm called SVR.

A set of data $T = \{(x_1,y_1), (x_2,y_2), \cdots, (x_n,y_n)\}$ is given, where $x_i \in R^n$, $y_i \in R^n$,$\{x_i, i = 1,2,\cdots,n\}$ is the input feature, $\{y_i, i = 1,2,\cdots,n\}$ is the output. The target of SVR method is to find a functional relationship similar to the hyperplane equation $f(x)$, making it as close to the training data as possible. In the feature space, the regression model corresponding to the hyperplane can be described as Eq. (5):

$$f(x) = \boldsymbol{w}_s{}^{\mathrm{T}}\varphi(x) + b_s \tag{5}$$

where $\varphi(x)$ is a nonlinear mapping function, $\boldsymbol{w}_s$ is the normal vector, b_s is the displacement term.

The optimization problem of SVR model can be expressed as:

$$\begin{aligned}&\min\ \frac{1}{2}\|\boldsymbol{w}_s\|^2 + C\sum\nolimits_{i=1}^{n}(\xi_i + \widehat{\xi}_i) \\ &\text{s.t.}\quad (\boldsymbol{w}_s{}^{\mathrm{T}}\varphi(x_i) + b_s - y_i) \le \varepsilon + \xi_i, \\ &y_i - \boldsymbol{w}_s{}^{\mathrm{T}}\varphi(x_i) - b_s \le \varepsilon + \widehat{\xi}_i,\ \xi_i \ge 0,\ \widehat{\xi}_i \ge 0,\ \ i = 1,2,\cdots,n\end{aligned} \tag{6}$$

where e is the regression error, similar to relaxation factor, which introduces outliers into the support vector. C is the penalty constant.

Four Lagrangian multipliers α_i, α_i*, u_i and u_i* are introduced to obtain Lagrangian function:

$$\begin{aligned}L(\boldsymbol{w}_s, b_s, \alpha_i, \alpha_i^*) = &\frac{1}{2}\|\boldsymbol{w}_s\|^2 + C\sum_{i=1}^{n}(\xi_i + \widehat{\xi}_i) - \sum_{i=1}^{n}\mu_i\xi_i - \sum_{i=1}^{n}\mu_i^*\widehat{\xi}_i \\ &+ \sum_{i=1}^{n}\alpha_i(\boldsymbol{w}_s{}^{\mathrm{T}}\cdot\varphi(x_i) + b_s - \xi_i - \varepsilon - y_i) + \sum_{i=1}^{n}\alpha_i^*(y_i - \boldsymbol{w}_s{}^{\mathrm{T}} \\ &\cdot\varphi(x_i) - b_s - \widehat{\xi}_i - \varepsilon)\end{aligned} \tag{7}$$

where $\alpha_i \ge 0$, α_i* $\ge$0, $u_i \ge 0$ and u_i* $\ge$0.

The SVR regression model can be finally transformed as the function below:

$$f(x) = \boldsymbol{w}_s{}^{\mathrm{T}}\cdot x + b_s = \sum_{i=1}^{n}\sum_{j=1}^{n}(\alpha_i^* - \alpha_i)K(x_i, x_j) + b_s \tag{8}$$

where $K(x_i, x_j)$ is the Gaussian radial basis kernel function, the expression of which is $K(x_i,x_j) = \exp\left(-\frac{\|x_i - x_j\|^2}{2\sigma^2}\right)$. The kernel function can improve the Feature dimension of the model to improve the nonlinear fitting ability of SVR. The larger the σ is, the smaller the nonlinear efficiency is, and the less sensitive to noise is.

When the amount of sample data is large, the distribution of high-dimensional feature space is uneven and there is heterogeneous information, a single selection of local kernel function or global kernel function will lead to low prediction accuracy. This problem can be solved by constructing multi-kernel functions by linear weighting.

By combining the linear kernel function with the Gaussian kernel function, the multi-kernel function can be expressed as:

$$K(x_i, x_j) = \lambda k_1(x_i, x') + (1 - \lambda)k_2(x_i, x') \tag{9}$$

where $k_1(x_i, x')$ is a linear kernel function, $k_2(x_i, x')$ is Gaussian kernel function. λ is the weight coefficient of linear kernel function, and the corresponding (1-λ) is the weight coefficient of Gaussian kernel function.

2.3. Improved sparrow search algorithm

The SSA is a new type of swarm intelligence optimization algorithm, and its basic structure is similar to ABC algorithm except the search operator [33]. In this paper, SSA algorithm is used to optimize penalty constant C and kernel function parameter σ to realize the accurate prediction of the MKSVM model.

For SSA algorithm, each sparrow has only one position, which can be represented by a matrix $\boldsymbol{X}$, and the expression is:

$$\boldsymbol{X} = \begin{bmatrix} x_{1,1} & x_{1,2} & \cdots & x_{1,d} \\ x_{2,1} & x_{2,2} & \cdots & x_{2,d} \\ \cdots & \cdots & \cdots & \cdots \\ x_{n,1} & x_{n,2} & \cdots & x_{n,d} \end{bmatrix} \tag{10}$$

where d is the dimension of the variable. $x_{i,j}$ indicates the position of the i-th sparrow in the j-th dimension.

The fitness value is calculated by:

$$\boldsymbol{F}_X = \begin{bmatrix} f([x_{1,1} & x_{1,2} & \cdots & x_{1,d}]) \\ f([x_{2,1} & x_{2,2} & \cdots & x_{1,d}]) \\ \cdots & & & \\ f([x_{n,1} & x_{n,2} & \cdots & x_{n,d}]) \end{bmatrix} \tag{11}$$

Each sparrow has three possible behaviors: explorer, follower, and vigilant investigation. Each generation selects the best P sparrows in the population as the explorers, and the remaining n-P sparrows as the followers.

The position update equation is:

$$X_{i,j}^{t+1} = \begin{cases} X_{i,j}^{t} \cdot \exp\left(\dfrac{-i}{\alpha \cdot M}\right), & R_2 < ST \\ X_{i,j}^{t} + Q_s \cdot \boldsymbol{L}_s, & R_2 \geq ST \end{cases} \tag{12}$$

where t is the number of current iteration, M is the maximum iterations number. $X_{i,j}^{t}$ indicates the position of the i-th sparrow in the j-th dimension of the current iteration. α is a random number between 0 and 1. R_2 is the alarm value and ST is the safety threshold. Q is a random number. $\boldsymbol{L}$ is a $1 \times d$ matrix with each element of 1.

The location updated equation is:

$$X_{i,j}^{t+1} = \begin{cases} \exp\left(\dfrac{X_{wp}^{t} - X_{i,j}^{t}}{i^2}\right) \cdot Q_s, & i > n/2 \\ \left|X_{i,j}^{t} - X_{bp}^{t+1}\right| \cdot \boldsymbol{G}_s^{+} \cdot \boldsymbol{L}_s + X_{bp}^{t+1}, & i \leq n/2 \end{cases} \tag{13}$$

where X_{bp} is the best position occupied by the current explorer, X_{wp} is the worst position. $\boldsymbol{G}$ represents a $1 \times d$ matrix with elements assigned 1 or -1 and $\boldsymbol{G}^{+} = \boldsymbol{G}^{T}(\boldsymbol{G}\boldsymbol{G}^{T})^{-1}$.

While the sparrows are foraging for food, part of them will be responsible for vigilance. When alerted to danger, they will conduct anti-predation behavior: give up food and move to a new location. The location update formula is:

$$X_{i,j}^{t+1} = \begin{cases} X_{bp}^{t} + \mu_s \cdot \left|X_{i,j}^{t} - X_{bp}^{t}\right|, & f_{si} > f_{sg} \\ X_{i,j}^{t} + K_s \cdot \left(\dfrac{\left|X_{i,j}^{t} - X_{wp}^{t}\right|}{(f_{si} - f_{sw}) + \xi}\right), & f_{si} = f_{sg} \end{cases} \tag{14}$$

where X_{bp} is the current global optimal position, μ_s is the step-size control parameter, K is the random with values between -1 and 1, which represents the moving direction of the sparrows. f_{si} is the fitness value of the current sparrow. f_{sg} represents current global best fitness value while f_{sw} represents the worst one. ξ is a minimum constant.

2.3.1. Improvement of population initialization

Elite chaotic opposition-learning method is adopted to generate an initial population to enhance its quality and diversity. By selecting elite individuals on a larger scale, the algorithm can improve the local escape ability and convergence performance of traditional SSA algorithm, then lead to a more accurate solution.

In this paper, the chaotic skew tent map is chosen to generate the initial population to enhance the stability of the initial individuals due to its characteristic of randomness and ergodicity.

The chaotic skew tent map equation is described as follows:

$$x_{k+1} = \begin{cases} x_k/\alpha, & 0 < x_k < \alpha \\ (1 - x_k)/(1 - \alpha), & \alpha < x_k \leq 1 \end{cases} \tag{15}$$

In Eq. (15), α is a random number between 0 and 1. $\beta = -\alpha\log\alpha-(1-\alpha)\log(1-\alpha)$, if $\beta > 0$, then the system is in chaos state.

The reverse-learning algorithm based on optical lens imaging principle can solve the problem of local optimum by increasing the probability of a better solution.

Reverse population generation equation is described in Eq. (16):

$$x_n^{*} = \frac{a_n + b_n}{2} + \frac{a_n + b_n}{2k} - \frac{x_n}{k} \tag{16}$$

where a_n represents the minimum value in the n dimension of the current population, while b_n represents the maximum one. k is the scaling coefficient of the lens.

The initialize process of the sparrow population with the strategy above is shown as follows:

Initialize the sparrow population randomly, then substitute population X into Eq. (15) to generate chaotic population Y. Generate the lens imaging opposition-learning population Z by substituting population X into Eq. (16). Sort the population X, Y and Z according to the individual fitness value and select the better N individuals to form the initial sparrow population.

2.3.2. Improvement of follower location update

Since the update weight is large and not changed much during iteration, it may miss the global optimum. To solve the problem, adaptive weights are introduced to improve the performance of SSA algorithm.

The changed update equation is described as follows:

$$X_{i,j}^{t+1} = \begin{cases} w_s \cdot \left(X_{i,j}^{t} \cdot \exp\left(\dfrac{-i}{\alpha_s \cdot Iter_{max}}\right)\right), & AR < ST \\ w_s \cdot \left(X_{i,j}^{t} + Q_s L_s\right), & AR \geq ST \end{cases} \tag{17}$$

$$w_s = 1 - \lg((e-1) \cdot n/Iter_{max} + 1)$$

2.4. A hybrid framework of VMD-ISSA-MKSVR

A hybrid framework combining VMD, ISSA and MKSVR model is proposed to achieve a more accurate and stable battery life prediction performance. The detailed prediction process is outlined in Fig. 1 (see Fig. 2).

The complete steps of the framework are summarized as follows.

Step 4. Some relevant features are extracted from current, voltage, and temperature curves. Then, features with high correlation are used as the input of VMD-ISSA-MKSVR model.

Step 5. Decompose the battery capacity by the VMD into 5 IMF components. Each component is processed to the VMD-ISSA-MKSVR model separately, and finally put it together.

Step 6. After VMD decomposition, ISSA algorithm is used to identify the parameters of MKSVR model.

Step 7. Train the VMD-ISSA-MKSVR model, and then substitute the test data into the training model for SOH estimation and RUL prediction results.

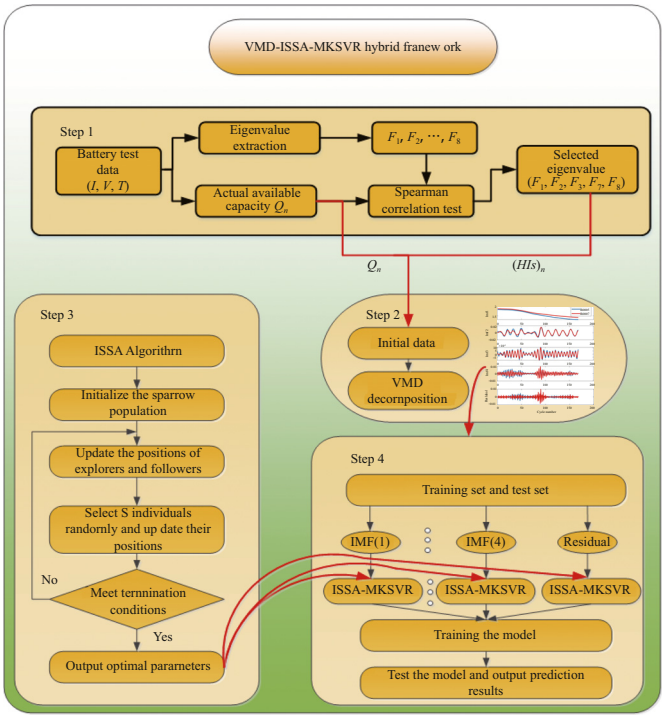

Fig. 1. Detailed flow chart of the hybrid framework.

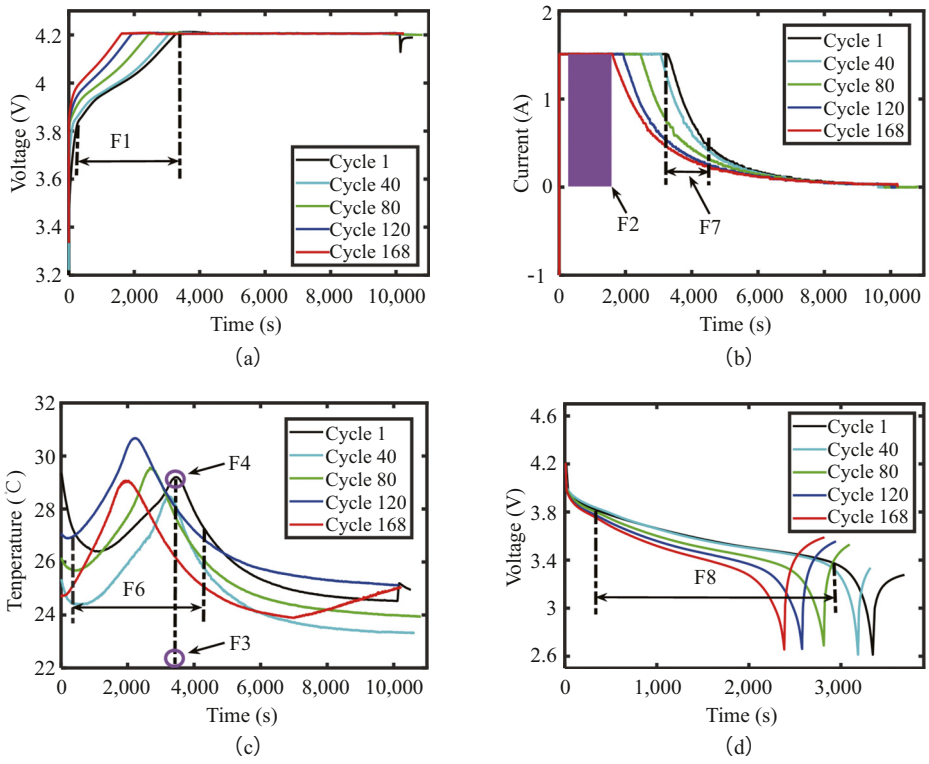

Fig. 2. Schematic diagram of extraction of eight eigenvalues at current, voltage and temperature. (a) F1. (b) F2 and F7. (c) F3, F4 and F6. (d) F8.

3. Experimental results and analysis

Four lithium-ion batteries (B0005, B0006, B0007 and B00018) from NASA are selected for SOH estimation and RUL prediction verification. The tests are carried out at room temperature, taking B0005 battery as an example: Charge the battery with a current of 1.5 A in a constant current (CC) mode until it reaches the charging cut-off voltage of 4.2 V. Then charge the battery by constant voltage (CV) mode with the voltage of 4.2 V, stop charging when the current drops to 0.02 A. During discharging, the battery is discharged in a CC mode, the discharging current is 2 A, stop discharging when the discharge cut-off voltage of 2.7 V is reached.

3.1. Evaluation criteria

For battery SOH estimation, this paper uses three popular criteria to verify the stability and accuracy of the model. Mean absolute error (MAE), root mean square error (RMSE), and mean absolute percentage error (MAPE) are adopted as evaluation criteria.

$$MAE = \frac{1}{M}\sum_{n=1}^{M}\left|y_n^* - y_n\right|$$

$$RMSE = \sqrt{\frac{1}{M}\sum_{n=1}^{M}\left(y_n^* - y_n\right)^2} \tag{18}$$

$$MAPE = \frac{1}{M}\sum_{n=1}^{M}\left|\frac{y_n^* - y_n}{y_n}\right| \times 100\%$$

Relative error (RE) is define as Eq. (19) for battery RUL prediction:

$$RE = \left|RUL_{\mathrm{p}} - RUL_{\mathrm{t}}\right| \tag{19}$$

where RUL_{p} is the predicted value of RUL, RUL_{t} is the actual value of RUL.

3.2. Feature extraction

The battery capacity cannot be obtained directly in practical. Some key features can be extracted from the current, voltage and temperature in the process of charging-discharging. It is easy to extract stable feature information from vehicle sensors to establish the relationship with battery SOH, and then use machine learning technology to realize battery life prediction.

In the process of battery operation, the voltage curve can provide a lot of information related to the available capacity. Time interval of equal charge voltage rise (TIE-CVR), charge capacity rise of equal charge voltage rise (CCR-CVR) and time interval of equal charge current drop (TIE-CCD) can be used as features to estimate battery SOH. TIE-CVR indicates the time for the voltage to rise from 3.8 V to 4.2 V during CC mode charging, which is marked as F1. The corresponding capacity of CCR-CVR is marked as F2. The highest temperature and the corresponding time in each charging–discharging cycle are marked as F3 and F4, respectively. During the period when the voltage is higher than 3.8 V and the current drops to 0.4 A, the average temperature is recorded as F5. The area under the temperature curve is recorded as F6. TIE-CCD is the time when the current in the CV phase decreases from 1.5 A to 0.4 A, which is marked as F7. During the period when the discharge voltage decreases from 3.8 V to 3.4 V, the capacity of the discharged battery is recorded as F8. Fig. 3 shows the eigenvalue of F1∼F8.

The spearman rank correlation coefficients R_S is used to analyze the correlation between eigenvalues and battery available capacity.

The formula is shown in Eq. (20):

$$R_S = \frac{\sum_{n=1}^{M}(X_n - \overline{X})(Y_n - \overline{Y})}{\sqrt{\sum_{n=1}^{M}(X_n - \overline{X})^2}\sqrt{\sum_{n=1}^{M}(Y_n - \overline{Y})^2}} \tag{20}$$

$$\overline{X} = \frac{1}{M}\sum\nolimits_{n=1}^{M} X_n$$

where X_n is the available capacity for each discharge, Y_n is the input eigenvalues in each charge–discharge cycle, $\overline{X}$ and $\overline{Y}$ are the mean values of

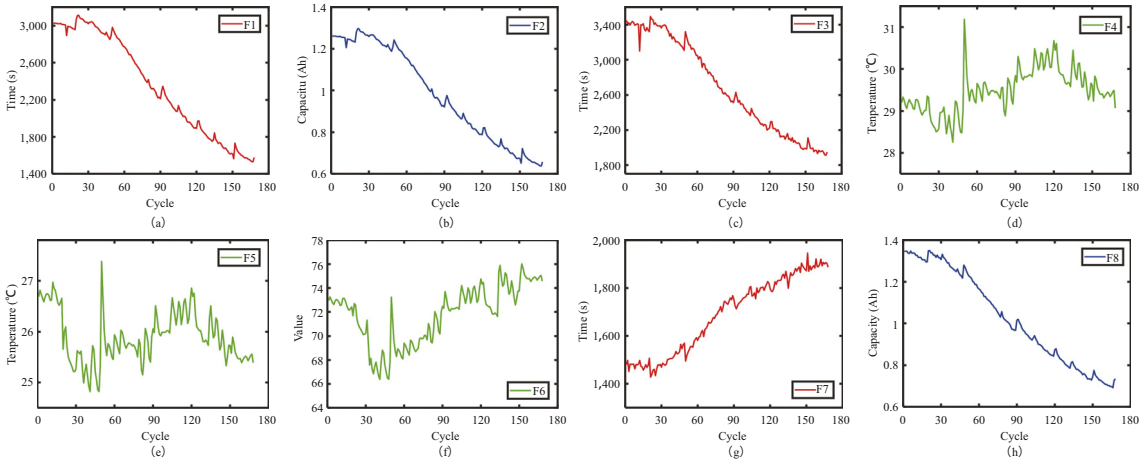

Fig. 3. The variation curve of eight characteristics (a)–(h) are F1–F8, respectively.

sample, n is the current charge–discharge cycle, M is the total number of charge and discharge cycles.

Table 1 depicts the correlation coefficient between each feature and available capacity.

Among the four batteries, the absolute values of the correlation coefficients between F1, F2, F3, F7, and F8 and the available capacity are all between 0.9 and 1, indicating a high correlation between them. The correlation values of eigenvalues F4, F5 and F6 with available capacity are all low, indicating that their correlation is also relatively low. These three features are eliminated, and not used as input to the estimation model.

3.3. SOH estimation

Before SOH estimation, the VMD method is used to decompose the data. The VMD decomposition diagram of B0005 and B0007 is shown in Fig. 4. Each data is divided into five components, The frequencies of five components are different. The component frequencies of B0005 and B0007 are similar.

In this paper, the capacity-based SOH definition method is adopted, which is defined as the ratio of the current capacity to the rated capacity of the battery. For the same battery, its rated capacity is constant, and the current capacity and SOH have the same trend. The problem of SOH estimation of the battery can be transformed into the problem of capacity estimation.

For SOH estimation, the characteristic factors are extracted as the input of VMD-ISSA-MKSVR model. The prediction start point of B0005, B0006 and B0007 is $Ty = 81$, while that of B00018 is $Ty = 61$. The data before the starting point is set as the training set, and the data after the starting point is set as the test set.

Four methods including the IPSO-SVR [34], ISSA-SVR, VMD-ISSA-SVR and BL-ELM [35] are in comparison with VMD-ISSA-MKSVR for

Table 1
Correlation coefficient between each feature and available capacity.

Battery number	Feature number							
	F1	F2	F3	F4	F5	F6	F7	F8
B0005	0.991,3	0.991,3	0.991,1	−0.588,0	0.071,7	−0.625,1	−0.981,9	0.998,7
B0006	0.993,6	0.993,6	0.991,5	−0.156,2	0.164,7	0.104,0	−0.952,2	0.999,2
B0007	0.988,8	0.988,8	0.989,7	−0.453,5	0.037,9	−0.071,2	−0.944,4	0.997,2
B0018	0.978,2	0.978,2	0.982,3	−0.263,1	0.708,4	0.212,7	−0.912,8	0.998,6

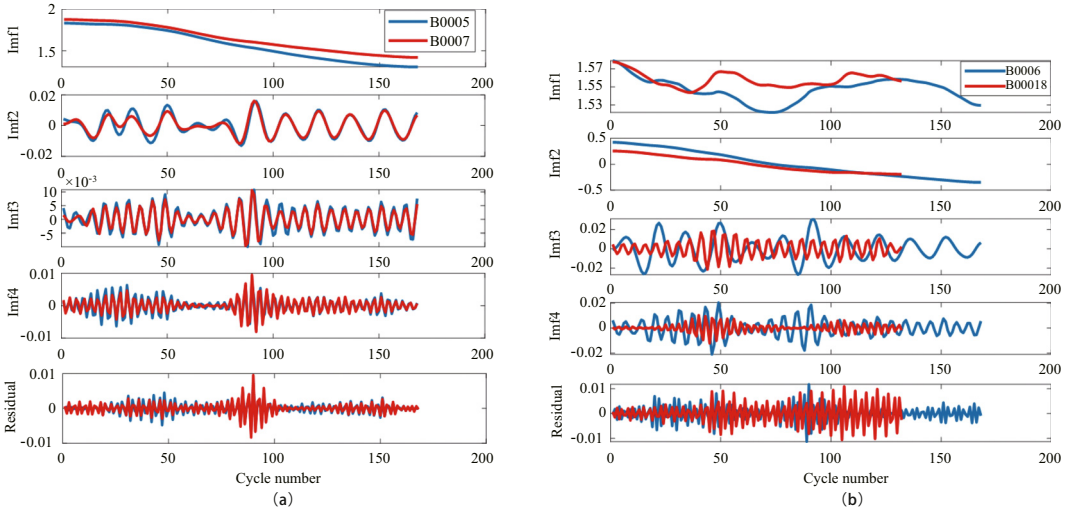

Fig. 4. Battery capacity estimation resultsVMD decomposition of capacity data. (a) B0005 and B0007. (b) B0006 and B00018.

battery SOH estimation. The relevant parameters are set in Table 2. The kernel parameters are Obtained by three optimization methods listed as Table 3.

To verify the effectiveness of the proposed method for SOH estimation, a comparison of the battery capacity estimation is conducted as shown in Fig. 5. The SOH estimation results clearly show that the conformance between estimation and measurement are adequate. The capacity estimation values all follow the actual value, and the errors are quite small. Compared with the capacity obtained by the IPSO-SVR and ISSA-SVR, that obtained by the VMD-ISSA-SVR and the VMD-ISSA-MKSVR are closer to the actual capacity.

The capacity estimation error is shown in Table 4 and Fig. 6. Take B0005 battery as an example, the MAE of the five methods are 2.160,3%, 0.708%, 0.651%, 0.647% and 0.489%, respectively, while the RMSE of that are 2.331%, 1.354%, 1.282%, 0.854% and 0.665%, respectively; and the MAPE of that are 1.345%, 0.508%, 0.470%, 0.455% and 0.346%, respectively. The capacity estimation error of the IPSO-SVR is largest, that of the proposed VMD-ISSA-MKSVR method is smallest, the error reductions of MAE, RMSE, and MAPE are obvious. Compared with the results predicted by the IPSO-SVR algorithm, the proposed method improves the estimation SOH accuracy by nearly 0.51%–2.11%. These results suggest that the proposed VMD-ISSA-MKSVR method has a relatively high estimation accuracy.

Table 2
The parameter setting.

Algorithm	Parameters
IPSO-SVR	$N = 100$, $Iter_{max} = 100$
ISSA-SVR	$N = 100$, $Iter_{max} = 100$
VMD-ISSA-SVR	$N = 100$, $Iter_{max} = 100$
BL-ELM	$N = 100$, $Iter_{max} = 100$
VMD-ISSA-MKSVR	$N = 100$, $Iter_{max} = 100$

Table 3
The kernel parameters are Obtained by three optimization methods.

Algorithm	B0005	B0006	B0007	B00018
IPSO-SVR	$\sigma = 0.01$	$\sigma = 0.01$	$\sigma = 0.01$	$\sigma = 0.01$
ISSA-SVR	$\sigma = 0.012{,}2$	$\sigma = 0.01$	$\sigma = 0.01$	$\sigma = 0.541{,}4$
VMD-ISSA-SVR	$\sigma = 404.72$	$\sigma = 337.7$	$\sigma = 1{,}386$	$\sigma = 512.9$

3.4. RUL prediction

The battery RUL prediction results are discussed in this section. Take the cycle number as input of the prediction methods, the EOL threshold for the B0005, B0006 and B00018 batteries are set to 70% of the standard rated capacity, which is 1.4 Ah. The EOL threshold for the B0007 battery is set to 75% of the standard rated capacity, which is 1.5 Ah. The prediction start points of the four batteries are $Ty = 41$.

Fig. 7 and Table 5 show the battery RUL prediction results. The RE of the proposed hybrid method is smaller than those of the other methods, indicating that the hybrid algorithm has a higher prediction accuracy.

Table 4
Battery capacity estimation error.

Battery	Algorithm	*MAE* (%)	*RMSE* (%)	*MAPE* (%)
B0005	IPSO-SVR [34]	2.160,3	2.331	1.345,3
	BL-ELM [35]	0.650,599	1.281,78	0.469,636
	ISSA-SVR	0.708,46	1.354,1	0.507,59
	VMD-ISSA-SVR	0.647,32	0.853,72	0.455,3
	VMD-ISSA-MKSVR	0.489,48	0.665,29	0.345,72
B0006	IPSO-SVR [34]	2.818	2.665,5	1.555,2
	BL-ELM [35]	0.907,669	1.897,84	0.692,424
	ISSA-SVR	0.932,02	2.019,6	0.713,44
	VMD-ISSA-SVR	0.847,19	1.277,6	0.640,3
	VMD-ISSA-MKSVR	0.701,88	1.075,7	0.531,36
B0007	IPSO-SVR [34]	0.944,4	1.608,6	0.559,21
	BL-ELM [35]	0.552,247	1.252,03	0.374,816
	ISSA-SVR	0.67	1.38	0.455
	VMD-ISSA-SVR	0.558,14	0.811,74	0.370,43
	VMD-ISSA-MKSVR	0.439,31	0.650,92	0.293,01
B00018	IPSO-SVR [34]	2.866,2	3.017,9	1.814
	BL-ELM [35]	1.277,36	2.009,69	0.896,704
	ISSA-SVR	2.269,7	2.510,5	1.576,9
	VMD-ISSA-SVR	1.640,7	1.348,9	0.937,12
	VMD-ISSA-MKSVR	1.271,3	1.100,8	0.882,36

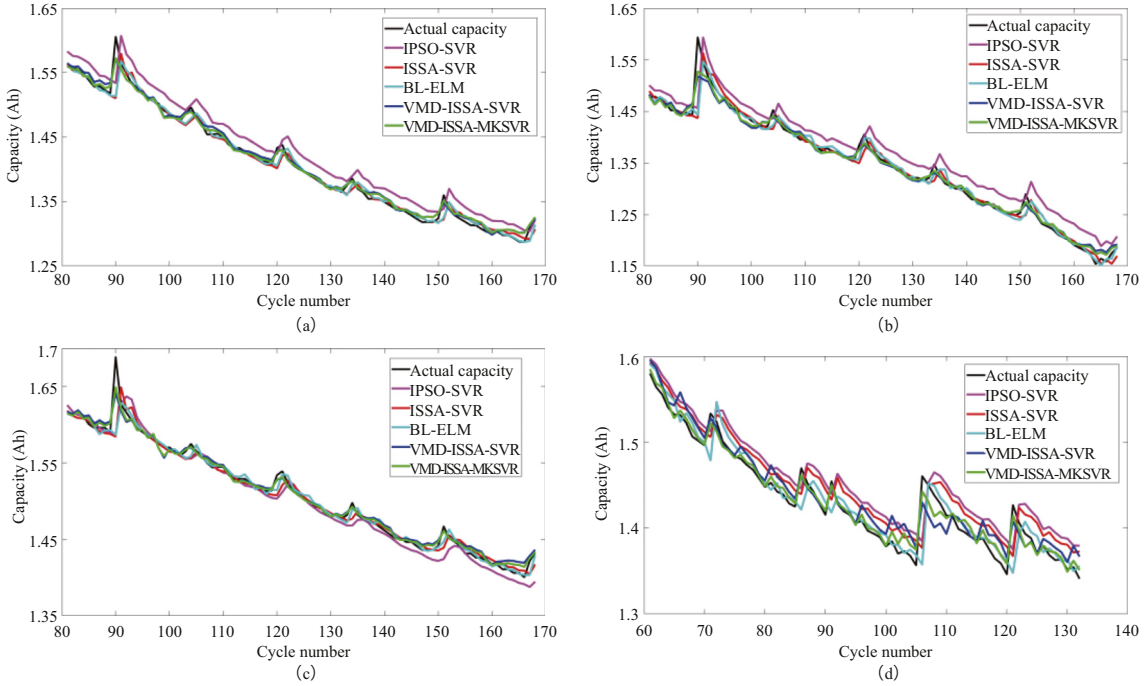

Fig. 5. Battery capacity estimation results. (a) B0005. (b) B0006. (c) B0007. (d) B00018.

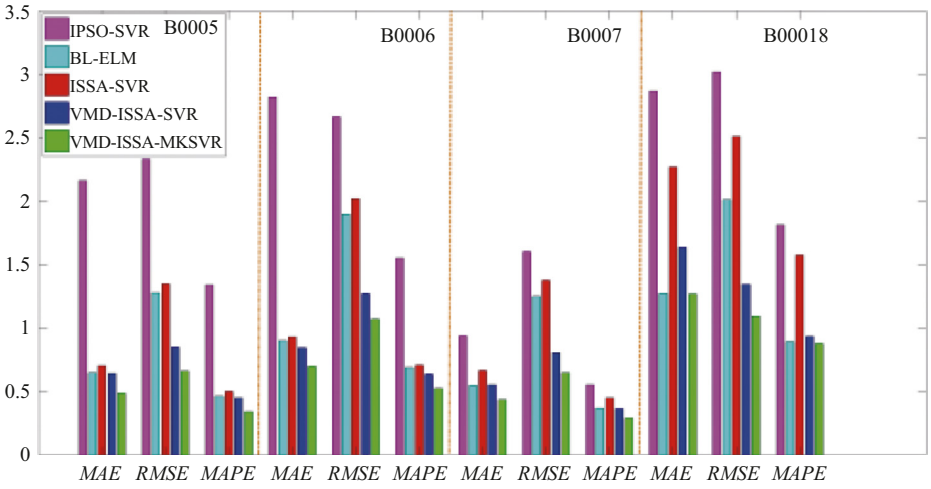

Fig. 6. Battery capacity estimation error.

The RE value predicted by the IPSO-SVR for four batteries are 12, 4, 7 and 11, respectively; by the BL-ELM method those are 5, 3, 6 and 11, respectively; by the ISSA-SVR method those are 6, 3, 7 and 10, respectively; by the VMD-ISSA-SVR method those are 3, 1, 5 and 8, respectively; by the VMD-ISSA-MKSVR method those are 1, 0, 0 and 3. Especially for B00018, the RUL prediction accuracy has been greatly improved.

The RUL prediction results of four batteries with different start points are shown in Table 6. ∞ in the table represents that the prediction curve and EOL do not intersect and the RUL cannot be predicted. It can be seen that the five methods can predict the RUL of the four batteries very well after $Ty = 41$ and the RE values obtained by the VMD-ISSA-MKSVR method are the smallest for every battery. The RE values predicted by the five methods generally show an roughly upward trend with the advancement of the start point. When $Ty = 31$, the RUL predictions of B0005 and B0007 batteries by IPSO-SVR and ISSA-SVR cannot be performed because of the small amount of data. The RUL errors predicted by BL-ELM, VMD-ISSA-SVR and VMD-ISSA-MKSVR are still suitable. With the advance of the start point, the prediction accuracy of the proposed hybrid method does not change much, indicating that the RUL predicted by VMD-ISSA-MKSVR method is stable.

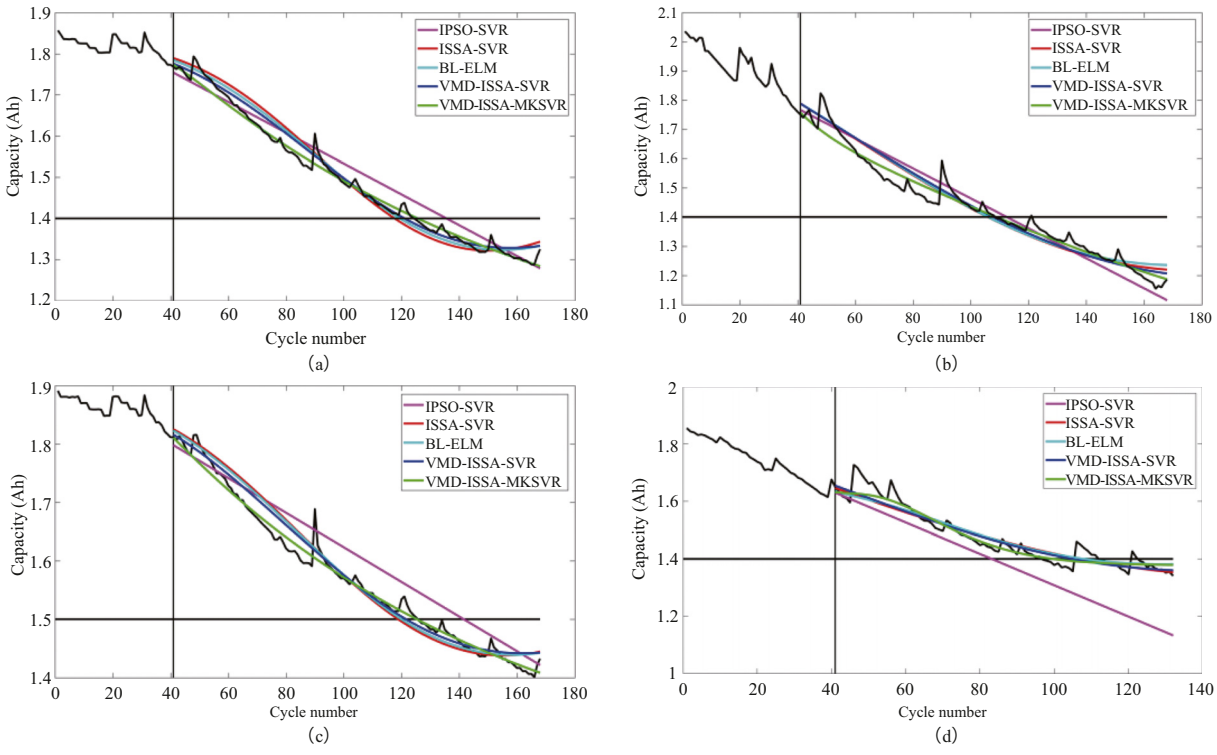

Fig. 7. Battery RUL prediction results. (a) B0005. (b) B0006. (c) B0007. (d) B00018.

Table 5
Battery RUL prediction error.

Battery	Algorithm	Start point	RUL_p	RUL_r	RE
B0005	IPSO-SVR [34]	41	95	83	12
	BL-ELM [35]	41	78	83	5
	ISSA-SVR	41	77	83	6
	VMD-ISSA-SVR	41	80	83	3
	VMD-ISSA-MKSVR	41	84	83	1
B0006	IPSO-SVR [34]	41	72	68	4
	BL-ELM [35]	41	65	68	3
	ISSA-SVR	41	65	68	3
	VMD-ISSA-SVR	41	67	68	1
	VMD-ISSA-MKSVR	41	68	68	0
B0007	IPSO-SVR [34]	41	92	85	7
	BL-ELM [35]	41	79	85	6
	ISSA-SVR	41	78	85	7
	VMD-ISSA-SVR	41	80	85	5
	VMD-ISSA-MKSVR	41	85	85	0
B00018	IPSO-SVR [34]	41	67	56	11
	BL-ELM [35]	41	67	56	11
	ISSA-SVR	41	66	56	10
	VMD-ISSA-SVR	41	64	56	8
	VMD-ISSA-MKSVR	41	59	56	3

Table 6
RUL prediction results of four batteries with different start points.

Battery	Algorithm	RE_{51}	RE_{41}	RE_{31}
B0005	IPSO-SVR [34]	10	12	∞
	BL-ELM [35]	8	5	20
	ISSA-SVR	10	6	∞
	VMD-ISSA-SVR	2	3	16
	VMD-ISSA-MKSVR	2	1	10
B0006	IPSO-SVR [34]	3	4	8
	BL-ELM [35]	6	3	23
	ISSA-SVR	4	3	9
	VMD-ISSA-SVR	2	1	10
	VMD-ISSA-MKSVR	1	0	2
B0007	IPSO-SVR [34]	8	16	∞
	BL-ELM [35]	7	6	8
	ISSA-SVR	6	7	∞
	VMD-ISSA-SVR	6	5	7
	VMD-ISSA-MKSVR	4	0	5
B00018	IPSO-SVR [34]	10	14	15
	BL-ELM [35]	13	11	9
	ISSA-SVR	12	10	10
	VMD-ISSA-SVR	9	8	6
	VMD-ISSA-MKSVR	2	3	1

4. Conclusion

As a key approach of prognostics and health management, accurate life prediction of the battery is significant to reduce the probability of system failure effectively. This work focus on a hybrid method considering feature extraction that combines VMD, ISSA and MKSVR.

The main contributions are summarized as follows: (1) eight features are extracted to establish the relationship with battery SOH by measured data; (2) decompose the original sequence by the VMD to solve the backward problem of the capacity data caused by auto-correlation to make the capacity data more stable; (3) elite chaotic opposition learning strategy and adaptive weights are introduced to optimize the SSA algorithm to find the global optimum faster and more efficient; (4) multi-Kernel support vector regression is used to solve the low prediction accuracy problem caused by large sample data, uneven distribution of high-dimensional feature space. Training data is used to train the hybrid model, and the test data is substituted into the training model for battery life prediction results.

Dataset from National Aeronautics and Space Administration are applied for experimental verification. The RUL predictions with different start points are conducted to verify the stability of the VMD-ISSA-MKSVR framework. By comparison with IPSO-SVR, ISSA-SVR, BL-ELM and VMD-ISSA-SVR, it can be verified that the errors of SOH estimation and RUL prediction obtained by the VMD-ISSA-MKSVR framework are the smallest. It has relatively high prediction accuracy and stability.

CRediT authorship contribution statement

Yuan Chen: conceptualization, methodology, software, validation, formal analysis, data curation, writing—original draft preparation.

Wenxian Duan: methodology, software, validation, formal analysis, writing—review and editing.

Yigang He: writing—supervision, funding acquisition.

Shunli Wang:writing—review and editing.

Carlos Fernandez:writing—review and editing

Data availability statement

The data and materials used to support the findings of this study are available from the corresponding author upon reasonable request.

Declaration of competing interest

The authors declare that they have no known competing financial interests or personal relationships that could have appeared to influence the work reported in this paper.

Acknowledgments

This work was supported by the National Natural Science Foundation of China (Grant number 51577046), the State Key Program of the National Natural Science Foundation of China (Grant number 51637004), and the National Key Research and Development Plan “Important Scientific Instruments and Equipment Development” (Grant number 2016YFF0102200).

References

[1] Wang, S., Fernandez, C., Yu, C., Fan, Y., Stroe, D. I. A novel charged state prediction method of the lithium ion battery packs based on the composite equivalent modeling and improved splice kalman filtering algorithm. J Power Sources, 471, 228450.
[2] Panchal S, Mathew M, Fraser R, Fowler M. Electrochemical thermal modeling and experimental measurements of 18650 cylindrical lithium-ion battery during discharge cycle for an EV. Appl Therm Eng 2018;135:123–32.
[3] Li P, Zhang Z, Xiong Q, Ding B, Hou J, Luo D, et al. State-of-health estimation and remaining useful life prediction for the lithium-ion battery based on a variant long short term memory neural network. J Power Sources 2020;459.
[4] Xiaoyu L, Zhang L, Wang Z. Remaining useful life prediction for lithium-ion batteries based on a hybrid model combining the long short-term memory and elman neural network. J Energy Storage 2019;21:510–8.
[5] Yl A, Kang LA, Xuan LA, Wang Y, Zhang L. Lithium-ion battery capacity estimation - a pruned convolutional neural network approach assisted with transfer learning. Appl Energy 2021;285:116410.
[6] Zheng Y, Qin C, Lai X, Han X, Xie Y. A novel capacity estimation method for lithium-ion batteries using fusion estimation of charging curve sections and discrete Arrhenius aging model. Appl Energy 2019;251:113327.
[7] Qin Q, Zhao S, Chen S, Huang D, Liang J. Adaptive and robust prediction for the remaining useful life of electrolytic capacitors. Microelectron Reliab 2018;87:64–74.
[8] Dong G, Chen Z, Wei J, Ling Q. Battery health prognosis using Brownian Motion modeling and particle filtering. IEEE Trans Ind Electron 2018;65(11):8646–55.
[9] Chang Y, Fang H. A hybrid prognostic method for system degradation based on particle filter and relevance vector machine. Reliab Eng Syst Saf 2019;186:51–63.
[10] Zhu ZY. Improved particle filter algorithm based on importance density function selection. In: Particle filter algorithm its application. 4nd ed. BeiJing, China: Science Press; 2010. p. 37–8.
[11] Wei JW, Dong GZ, Chen ZH. Remaining useful life prediction and state of health diagnosis for lithium-ion batteries using particle filter and support vector regression. IEEE Trans Ind Electron 2018;65(7):5634–43.
[12] Mejdoubi AE, Chaoui H, Gualous H. Lithium-ion batteries health prognosis considering aging conditions. IEEE Trans Power Electron 2019;34:6834–44.
[13] Chen Y, He YG, Li Z, Chen L, Zhang C. Remaining useful life prediction and state of health diagnosis of lithium-ion battery based on second-order central difference particle filter. IEEE ACESS 2020;8:37305–13.

[14] Li QL, Li DZ, Zhao K, Wang L, Wang K. State of health estimation of lithium-ion battery based on improved ant lion optimization and support vector regression. J Energy Storage 2022;50:104215.
[15] Pang X, Huang R, Wen J, Shi Y, Jia J, Zeng J. A lithium ion battery RUL prediction method considering the capacity regeneration phenomenon. Energies 2019;12(12).
[16] Yang H, Wang P, An Y, Shi C, Sun X, Wang K, et al. Remaining useful life prediction based on denoising technique and deep neural network for lithium-ion capacitors. eTransportation 2020;5:100078.
[17] Li W, Jiao Z, Du L, Fan W, Zhu Y. An indirect RUL prognosis for lithium-ion battery under vibration stress using Elman neural network. Int J Hydrogen Energy 2019; 44(23):12270–6.
[18] Wang S, Yongcun F, Siyu J, Paul T, Carlos F. Improved anti-noise adaptive long short-term memory neural network modeling for the robust remaining useful life prediction of lithium-ion batteries. Reliab Eng Syst Saf 2023;230:108920.
[19] Li L, Liu Z, Tseng M, Chiu A. Enhancing the Lithium-ion battery life predictability using a hybrid method. Appl Soft Comput 2019;74:110–21.
[20] Mengyun Z, Wang S, Yanxin X, Yang X, Hao X, Carlos F. Hybrid gray wolf optimization method in support vector regression framework for highly precise prediction of remaining useful life of lithium-ion batteries. Ionics 2023;29(9).
[21] Li X, Yuan C, Wang Z. State of health estimation for Li-ion battery via partial incremental capacity analysis based on support vector regression. Energy 2020;203:117852.
[22] Feng X, Weng C, He X, Han X, Lu L, Ren D, et al. Online state-of-Health estimation for li-ion battery using partial charging segment based on support vector machine. IEEE Trans Veh Technol 2019;68(9):8583–92.
[23] Zhang S, Zhai B, Guo X, Wang K, Peng N, Zhang X. Synchronous estimation of state of health and remaining useful lifetime for lithium-ion battery using the incremental capacity and artificial neural networks. J Energy Storage 2019;26: 100951.1–100951.12.
[24] Zhao, Qin Qi, Zhao H, Feng W. A novel prediction method based on the support vector regression for the remaining useful life of lithium-ion batteries. Microelectron Reliab 2018;85:99–108.
[25] Cadini F, Sbarufatti C, Cancelliere F, Giglio M. State-of-life prognosis and diagnosis of Lithium-ion batteries by data-driven particle filters. Appl Energy 2019;235: 661–72.
[26] Zhao L, Wang Y, Cheng J. A hybrid method for remaining useful life estimation of Lithium-ion battery with regeneration phenomena. Appl Sci 2019;9(9):1890–905.
[27] Li F, Xu J. A new prognostics method for state of health estimation of Lithium-ion batteries based on a mixture of Gaussian process models and particle filter. Microelectron Reliab 2015;55(7):1035–45.
[28] Qin T, Zeng S, Guo J. Robust prognostics for state of health estimation of lithium-ion batteries based on an improved PSO-SVR model. Microelectron Reliab 2015; 55(9–10):1280–4.
[29] Wang Y, Ni Y, Lu S, Wang J, Zhang X. Remaining useful life prediction of Lithium-ion batteries using support vector regression optimized by artificial bee colony. IEEE Trans Veh Technol 2019;68(10):9543–53.
[30] Li X, Zhang L, Wang Z, Dong P. Remaining useful life prediction for lithium-ion batteries based on a hybrid model combining the long short-term memory and Elman neural networks. J Energy Storage 2019;21:510–8.
[31] Jiang Y, Chen L, Zeng W, Xin Y. Adaptive weighted VMD-WPEE method of power-electronic-circuit multiple-parameter-fault diagnosis. IEEE J Emerg Selec Topics Power Electr 2020;(99):3878–90.
[32] Shi W, Wen G, Huang X, Zhang Z, Zhou Q. VMD-scale space based hoyergram and its application in rolling bearing fault diagnosis. Measurement Science and Technology 2020.
[33] Xue J, Shen B. A novel swarm intelligence optimization approach: sparrow search algorithm. Sys Sci Contr Eng Open Access J 2020;8(1):22–34.
[34] Qin T, Zeng S, Guo J. Robust prognostics for state of health estimation of lithium-ion batteries based on an improved PSO-SVR model. Microelectron Reliab 2015;55: 1280–4.
[35] Ma Y, Wu L, Guan Y, Peng Z. The capacity estimation and cycle life prediction of lithium-ion batteries using a new broad extreme learning machine approach. J Power Sources 2020;476:228581.